Minding the Gap between Hard and Diffractive Structure Functions at the Electron-Ion Collider

June-Haak Ee,[1,2,*] Christopher Lee,[2,3,†] and Stella T. Schindler[2,3,‡]
[1]MIT Center For Theoretical Physics—A Leinweber Institute, Cambridge, Massachusetts 02139, USA
[2]Theoretical Division, Los Alamos National Laboratory, Los Alamos, New Mexico 87545, USA
[3]Physics Division, Los Alamos National Laboratory, Los Alamos, New Mexico 87545, USA

(Received 20 July 2026; revised 27 September 2026; accepted 26 October 2026; published 19 November 2026)

Diffraction is characterized by forward scattering and a large rapidity gap. Ordinary hard scattering also produces gapped events and presents a significant background to identification of diffractively produced events. We present a fully differential factorization of gapped hard ep scattering. We find that the unpolarized azimuthally dependent structure functions $F_{3,4}^{\mathrm{gap}}$ and the longitudinal F_L^{gap} vanish at leading power for hard scattering. Azimuthal dependence is thus a pure diffractive signature. This is borne out in Monte Carlo simulations.

DOI: 10.1103/7jkz-3r9q

Twenty percent of collisions at the upcoming Electron-Ion Collider (EIC) at Brookhaven are expected to exhibit a strange feature: a large angular wedge of the detector (a *rapidity gap*) will remain untouched by the particle spray [1]. Rapidity-gapped events that involve a forward-scattered initial-state hadron are called *diffractive* [2–4]. Diffraction is among the cleanest probes of gluon saturation [5,6], and illuminates physics ranging from forward (Regge) dynamics [7] to cosmic-ray cascades [8,9] and beyond-the-standard-model dynamics [10–13].

A rapidity gap, however, does not by itself signal diffraction. Large gaps also arise in ordinary hard scattering [14–31], e.g., when a pencil-like two-jet configuration leaves the central region empty. This mechanism is distinct from the forward exchange of diffraction. Because the gap itself often has served as the experimental criterion for selecting diffractive events [32] (particularly for *incoherent* diffraction, which produces a forward jet), this hard component is an irreducible background that can bias diffractive measurements, and hence the physics extracted from them. The two are hardest to tell apart precisely where the contamination matters most: in large-gap events.

In this Letter, we provide a fully differential *factorization formula* for hard ep scattering with two gapped rapidity sectors (Fig. 1), expressing its cross section in terms of first-principles field theory operators. A typical gap choice is $\Delta\eta \gtrsim 2$–3 [33,34]. The formula predicts both the rate of gapped hard events and their contamination of diffractive observables. Our central result is that the structure functions F_L^{gap}, F_3^{gap}, and F_4^{gap} vanish at leading power in gapped hard scattering: the hard tensor is azimuthally trivial, so the azimuthal structure functions $F_{3,4}^{\mathrm{gap}}$—and the longitudinal F_L^{gap}—are pure diffractive signatures in the presence of a gap. Measuring azimuthal dependence therefore cleanly separates genuine diffraction from its hard background. We perform Monte Carlo simulations with RAPGAP [35] which show that the hard $F_{3,4}^{\mathrm{gap}}$ switch off in the large-gap limit, leaving azimuthal dependence as a clean diffractive signature.

Kinematics—Consider the gapped process $ep \to e' X_C X_T$ in Fig. 1, where X_C and X_T are sprays of one or more particles (e.g., a jet) in the central and target regions, separated by a rapidity gap. The initial and final electrons carry momenta k and k', while the initial proton and final hadronic state X_T carry momenta p and p', respectively. The lepton and hadron transfer momenta $q = k - k'$ and $\tau = p - p'$ to the central system X_C, which carries momentum $p_X = q + \tau$.

We work with vanishing hadronic and leptonic mass $k^2 = k'^2 = m_e^2 \approx 0$ and $p^2 = m_p^2 \approx 0$ giving seven independent Lorentz invariants:

$$x = \frac{Q^2}{2p\cdot q}, \qquad y = \frac{p\cdot q}{p\cdot k}, \qquad Q^2 = -q^2,$$
$$\beta = \frac{Q^2}{2q\cdot\tau}, \qquad t = \tau^2, \qquad \bar{x} = \frac{k\cdot\tau}{k\cdot p}, \qquad m_T^2 = (p')^2. \tag{1}$$

*Contact author: jhee@mit.edu
†Contact author: clee@lanl.gov
‡Contact author: schindler@lanl.gov

Published by the American Physical Society under the terms of the Creative Commons Attribution 4.0 International license. Further distribution of this work must maintain attribution to the author(s) and the published article's title, journal citation, and DOI. Funded by SCOAP³.

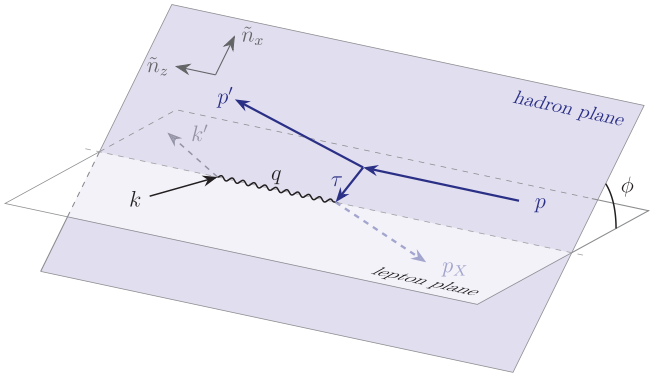


FIG. 1. Breit frame configuration of gapped hard scattering $ep \to e' X_C X_T$, with X_i a collection of one or more particles. The lepton plane (with k, k', q) and hadron plane (with p, p', p_X, τ) intersect along q and are separated by azimuthal angle ϕ. The longitudinal ($\tilde{n}_z$) and transverse ($\tilde{n}_x$, in hadron plane) axes are indicated.

It is often useful to consider additional invariants that are not independent of the above:

$$W^2 = (p+q)^2 = Q^2\frac{1-x}{x}, \qquad s = (p+k)^2 = \frac{Q^2}{xy},$$
$$m_X^2 = p_X^2 = Q^2\frac{1-\beta}{\beta} + t, \qquad z = \frac{p\cdot p'}{p\cdot q} = \frac{x}{Q^2}(m_T^2 - t). \tag{2}$$

Reference [36] provides bounds for these invariants.

Breit frame—We work in the Breit frame, defined as

$$p^\mu = \frac{Q}{x}\frac{n^\mu}{2}, \qquad q^\mu = Q\frac{\bar{n}^\mu - n^\mu}{2}, \tag{3}$$

up to mass corrections $\sim\mathcal{O}(m_p^2/Q^2)$. In this frame, the lightlike vectors n and $\bar{n}$ are $n^\mu = (2/Q)xp^\mu$ and $\bar{n}^\mu = (2/Q)(xp^\mu + q^\mu)$. Then, defining the light-cone coordinates $p^\mu = (n\cdot p, \bar{n}\cdot p, p_\perp)$, we have $n^\mu = (0, 2, 0_\perp)$ and $\bar{n}^\mu = (2, 0, 0_\perp)$, and

$$\tau = Q\left(-z, \frac{1}{\beta} - z, -\sqrt{z^2 - z/\beta - t/Q^2}\right),$$
$$p_X = Q\left(1-z, \frac{1-\beta}{\beta} - z, -\sqrt{z^2 - z/\beta - t/Q^2}\right),$$
$$p' = Q\left(z, \frac{1}{x} - \frac{1}{\beta} + z, \sqrt{z^2 - z/\beta - t/Q^2}\right). \tag{4}$$

The transverse axis is taken in the hadron plane (Fig. 1), with p' at positive $\perp$ and the recoil τ, p_X at negative $\perp$.

Structure functions—Following [36], the fully differential cross sections for diffraction and gapped hard scattering both take the form

$$\frac{d^6\sigma}{dxdQ^2d\beta dtdm_T^2d\phi} = \frac{\pi\alpha^2xy^2}{4Q^6\beta^2}L_{\mu\nu}(k,k')W^{\mu\nu}_{\text{gap}}(q,p,p'), \tag{5}$$

where ϕ is the relative azimuthal angle of p' with respect to the lepton plane. The unpolarized leptonic and hadronic tensors are

$$L^{\mu\nu} = 2(k^\mu k'^\nu + k^\nu k'^\mu - k\cdot k' g^{\mu\nu}),$$
$$W^{\mu\nu}_{\text{gap}} = \sum\!\!\!\!\!\!\int_{X_C,X_T} \delta^4(q+p-p'-p_X)\delta(m_T^2 - p'^2) \times \langle p|J^{\dagger\mu}(0)|X_CX_T\rangle\langle X_CX_T|J^\nu(0)|p\rangle, \tag{6}$$

with the vector current $J^\mu = \sum_f e_f\bar{\psi}_f\gamma^\mu\psi_f$ for quark flavors f of charge e_f, and each phase-space sum and integral $\sum\!\!\!\!\!\!\int$ running over all final-state configurations, with $\sum\!\!\!\!\!\!\int_{X_T}$ normalized to 1 for the one-particle X_T state. We work throughout in the unpolarized, vector-vector case: electromagnetic currents dominate in the moderate $x = Q^2/sy$ kinematics at the EIC ($\sqrt{s} = 20$–140 GeV) and HERA ($\sqrt{s} = 319$ GeV) on which we focus.

As in [36,37], we decompose $W^{\mu\nu}_{\text{gap}}$ into structure functions F_i^{gap},

$$W^{\mu\nu}_{\text{gap}} = \sum_i w_i^{\mu\nu}(U,X,Z)F_i^{\text{gap}}(x,Q^2,\beta,t,m_T^2), \tag{7}$$

with $i \in \{L, 2, 3, 4\}$. These F_i^{gap} have dependence on p' through the invariants in Eq. (1), unlike the structure functions F_i of DIS. Here U^μ, X^μ, Z^μ are orthonormal vectors:

$$U^\mu = \frac{2x}{Q}\left(p^\mu + \frac{q^\mu}{2x}\right),$$
$$X^\mu = \frac{\left(\frac{1}{\beta} - 2z\right)xp^\mu - zq^\mu - \tau^\mu}{Q\sqrt{z^2 - z/\beta - t/Q^2}}, \quad Z^\mu = -\frac{q^\mu}{Q}, \tag{8}$$

which satisfy $U^2 = 1$, $X^2 = Z^2 = -1$ and $U\cdot X = U\cdot Z = Z\cdot X = 0$. In the Breit frame, $X^\mu = \tilde{n}_x^\mu = (0,1,0,0)$ and $Z^\mu = \tilde{n}_z^\mu = (0,0,0,1)$ are the transverse and longitudinal spatial axes shown in Fig. 1, while $U^\mu = \tilde{n}_t^\mu = (1,0,0,0)$ is the time direction. Defining the remaining spacelike direction normal to the hadron plane (not shown in Fig. 1),

$$Y^\mu = \epsilon^{\mu\nu\rho\sigma}U_\nu X_\rho Z_\sigma, \qquad Y^2 = -1, \tag{9}$$

which in the Breit frame is $Y^\mu = \tilde{n}_y^\mu = (0,0,1,0)$, the four vectors form a complete orthonormal basis (with U timelike) valid in any frame:

$$g^{\mu\nu} = U^\mu U^\nu - X^\mu X^\nu - Y^\mu Y^\nu - Z^\mu Z^\nu. \tag{10}$$

The tensors $w_i^{\mu\nu}$ are then constructed from these basis vectors as

$$\begin{aligned} w_L^{\mu\nu} &= 1/(2x)(U^\mu U^\nu - X^\mu X^\nu - Y^\mu Y^\nu), \\ w_2^{\mu\nu} &= 1/(2x)(X^\mu X^\nu + Y^\mu Y^\nu), \\ w_3^{\mu\nu} &= 1/(2x)(X^\mu X^\nu - Y^\mu Y^\nu), \\ w_4^{\mu\nu} &= 1/(2x)(U^\mu X^\nu + X^\mu U^\nu), \end{aligned} \tag{11}$$

where we use the completeness relation in Eq. (10). These have projectors $\mathcal{P}_i$ satisfying $\mathcal{P}_{i\mu\nu} w_j^{\mu\nu} = \delta_{ij}$ (see Ref. [36]), so that $\mathcal{P}_{i\mu\nu} W_{\rm gap}^{\mu\nu} = F_i^{\rm gap}$. The azimuthal functions $F_{3,4}^{\rm gap}$ probe the X-Y anisotropy of $W_{\rm gap}^{\mu\nu}$, which we show below vanish at leading power in hard scattering. Note that the diffractive naming convention [36] for these parity-conserving $F_{3,4}^{\rm gap}$ is distinct from the traditional parity-violating structure function F_3 of DIS.

In the Breit frame, the azimuthal angle ϕ of $p'_\perp$ about q, measured from the lepton plane (Fig. 1), is fixed by

$$\begin{aligned} k \cdot X &= k \cdot \tilde{n}_x = -|k_\perp| \cos\phi, \\ k \cdot Y &= k \cdot \tilde{n}_y = -|k_\perp| \sin\phi, \end{aligned} \tag{12}$$

where the minus signs arise from the spacelike metric. Then, from $|k_\perp| = Q\sqrt{1-y}/y$ in the Breit frame and the explicit expression for X^μ in Eq. (8), we can write $\cos\phi$ in terms of Lorentz invariants as

$$\cos\phi = \frac{\bar{x} - x/\beta + (2-y)xz}{2x\sqrt{1-y}\sqrt{z^2 - z/\beta - t/Q^2}}. \tag{13}$$

The leptonic-hadronic contraction then becomes

$$\begin{aligned} L_{\mu\nu} W_{\rm gap}^{\mu\nu} = \frac{2s}{y}\Bigg[&-\frac{y^2}{2} F_L^{\rm gap} + \left(1 - y + \frac{y^2}{2}\right) F_2^{\rm gap} \\ &+ (1-y)\cos(2\phi) F_3^{\rm gap} - (2-y)\sqrt{1-y}\cos\phi F_4^{\rm gap}\Bigg]. \end{aligned} \tag{14}$$

For diffractive kinematics, $F_2^{\rm gap}$ was measured often at HERA; $F_L^{\rm gap}$ less so [38]. Measuring $F_{3,4}^{\rm gap}$ would require sufficient resolution in $\bar{x}$; see Sec. 2.4 of [36] and [39].

Kinematic constraints—We now quantify what rapidity-gapped hard scattering requires kinematically. First, the ep collision must be hard; second, p' and p_X must form two distinct, low-mass hadronic sectors; third, there must be a rapidity gap between them, with $\eta(k) = \frac{1}{2}\ln(k^-/k^+)$, $k^+ = n \cdot k$, $k^- = \bar{n} \cdot k$. These give

$$x \sim 1, \qquad \Lambda_{\rm QCD}^2 \ll m_X^2,\, m_T^2 \ll Q^2, \qquad \frac{p_X^-}{p_X^+} \ll \frac{p'^-}{p'^+}. \tag{15}$$

Their consequences for the invariants are immediate: combining $x \sim 1$ with $m_X^2 \ll Q^2$ gives $1 - \beta \ll 1$, whence $-t = Q^2(1-\beta)/\beta - m_X^2 \ll Q^2$. The full set of conditions for gapped hard scattering and diffraction [36] is collected in Table I.

We encode these scalings in *power-counting* parameters

$$\lambda = \frac{Q}{\sqrt{s}}, \qquad \lambda_t = \frac{\sqrt{-t}}{Q}, \qquad \rho = \frac{m_T}{\sqrt{-t}}, \qquad \lambda_\Lambda = \frac{\Lambda_{\rm QCD}}{\sqrt{-t}}, \tag{16}$$

in terms of which the constraints read

$$\lambda \sim 1, \qquad \lambda_t \ll 1, \qquad \lambda_t \rho \ll 1, \qquad \lambda_\Lambda \ll 1, \tag{17}$$

together with $1 - \beta \ll 1$. We can then express the Breit-frame momenta in terms of their scaling in λ_t:

$$\begin{aligned} p &\sim \sqrt{s}(0,1,0), & q &\sim \sqrt{s}(1,1,0), \\ p_X &\sim \sqrt{s}(1,\lambda_t^2,\lambda_t), & \tau &\sim \sqrt{s}(\lambda_t^2,1,\lambda_t), \\ p' &\sim \sqrt{s}(\lambda_t^2,1,\lambda_t). \end{aligned} \tag{18}$$

Here, we drop $\mathcal{O}(\lambda_\Lambda)$ terms and consider $1 - \beta \sim \lambda_t^2$, $\rho \sim 1$ for simplicity: Eq. (17) indicates that analyzing the hard interaction will require us to expand in $\lambda_t \ll 1$, but does not require such an expansion for the other parameters.

Equation (18) enables us to *factorize* $W_{\rm gap}^{\mu\nu}$, i.e., to separate the physics of different momentum scales into field theory matrix elements with clear physical interpretation. We use the technique of *effective field theory* (EFT), which systematically power expands the QCD Lagrangian in $\lambda_t \ll 1$ about relevant modes. The modes in Eq. (18) belong to the soft-collinear effective theory (SCET) [40–44]: p, τ, p' are n collinear, p_X is $\bar{n}$ collinear, and the exchanged photon q is hard. Note that these modes can also radiate ultrasoft modes of momentum scaling $\sim\sqrt{s}(\lambda_t^2, \lambda_t^2, \lambda_t^2)$ without changing the invariant mass scaling of $X_{T,C}$, whereas soft modes $\sim\sqrt{s}(\lambda_t, \lambda_t, \lambda_t)$ would; the

TABLE I. Behavior of Lorentz invariants, defined in Eqs. (1) and (2), in gapped hard scattering vs diffraction with two measured final-state regions separated by a rapidity gap [36].

Invariant	Gapped hard	Diffraction
x	$x \sim \mathcal{O}(1)$	$x \ll 1$
β	$1 - \beta \ll 1$	$\beta \gg x$, with $\beta \sim 1$ or $\beta \ll 1$
m_X, m_T	$m_X^2, m_T^2 \ll Q^2$	$m_X^2, m_T^2 \ll W^2$
t	$-t \ll Q^2 \sim s$	$-t \ll W^2$

mass measurements thus select ultrasoft radiation, which we must build into our formalism.

Factorization—The factorization of $W^{\mu\nu}_{\rm gap}$ in Eq. (6) closely parallels the fully differential form of the 1-jettiness factorization of Ref. [14], which likewise describes hard scattering with two rapidity-separated sectors. We sketch its structure here, and provide a complete derivation in Supplemental Material [45].

Using SCET, the states in Eq. (6) factorize into n-collinear, $\bar{n}$-collinear, and ultrasoft (us) components:

$$\langle p| = \langle p_n|\langle 0_{\bar{n}}|\langle 0_{us}|, \qquad |X_C X_T\rangle = |0_{us}\rangle|X_{C,\bar{n}}\rangle|X_{T,n}\rangle. \tag{19}$$

The electromagnetic current matches onto a hard coefficient $\mathcal{C}^\nu$ connecting the n-collinear (beam) and $\bar{n}$-collinear (current) sectors, $J^\nu \to \sum_f e_f \bar{\chi}_{\bar{n}} \mathcal{C}^\nu \chi_n$, with χ_n the n-collinear quark field in SCET. Decoupling collinear and ultrasoft fields by the standard BPS field redefinition [43], $\chi_n \to Y_n \chi_n$ with Y_n an ultrasoft gluon Wilson line, gives

$$J^\nu = \sum_f e_f \mathcal{C}^\nu \bar{\chi}_{\bar{n}} T[Y^\dagger_{\bar{n}} Y_n]\chi_n. \tag{20}$$

Inserting Eqs. (19) and (20) into Eq. (6), we have schematically that, up to subleading corrections in λ_t,

$$W^{\mu\nu}_{\rm gap}(q,p,p') = \mathcal{C}^\nu \mathcal{C}^\mu \sum_{X_C} \langle 0_{\bar{n}}|\chi_{\bar{n}}|X_{C,\bar{n}}\rangle\langle X_{C,\bar{n}}|\bar{\chi}_{\bar{n}}|0_{\bar{n}}\rangle \times \sum_{X_T} \langle p_n|\bar{\chi}_n|X_{T,n}\rangle\langle X_{T,n}|\chi_n|p_n\rangle \delta(m_T^2 - p'^2)$$
$$\times \langle 0_{us}|\bar{T}[Y^\dagger_n Y_{\bar{n}}]T[Y^\dagger_{\bar{n}} Y_n]|0_{us}\rangle \delta^4(q + p - p' - p_X), \tag{21}$$

where we have preemptively grouped terms of the same scaling together and collected $\sum_f e_f^2$ into the hard coefficients. This simplifies to

$$W^{\mu\nu}_{\rm gap} = H^{\mu\nu} \otimes \mathcal{B} \otimes J \otimes S, \tag{22}$$

where the hard (H), beam ($\mathcal{B}$), jet (J), and soft functions are, schematically,

$$H^{\mu\nu} = \mathcal{C}^\nu \mathcal{C}^\mu, \qquad \mathcal{B} = \langle p_n|\bar{\chi}_n \chi_n|p_n\rangle,$$
$$J = \langle 0|\chi_{\bar{n}}\bar{\chi}_{\bar{n}}|0\rangle, \qquad S = \langle 0|\bar{T}[Y^\dagger_n Y_{\bar{n}}]T[Y^\dagger_{\bar{n}} Y_n]|0\rangle. \tag{23}$$

The gap measurements enter as δ functions fixing the sector virtualities: the jet virtuality follows internally as $m_X^2 = Q^2(1-\beta)/\beta + t$, entering the jet function J, while $\mathcal{B}$ coincides with the standard 1-jettiness fully differential beam function, with its arguments fixed by the m_T^2 and t measurement δ functions. The shared soft momenta thread S, assembling the fully differential cross section. (See Supplemental Material [45] for the full expression.) Imposing genuinely new constraints—e.g., a further rapidity gap within a sector, taking an exclusive final state, or a different ρ scaling—can refactorize J or $\mathcal{B}$ into additional matrix elements. All Lorentz indices reside in $H^{\mu\nu}$, which we turn to next.

Vanishing structure functions—Since $H^{\mu\nu}$ carries all the Lorentz indices of Eq. (22), the structure-function content is fixed by its tensor structure alone. At leading power, for the vector-vector currents of Eq. (6), Ref. [14] gives $H^{\mu\nu} = -g_\perp^{\mu\nu} H(Q^2,\mu)$ with a scalar coefficient $H(Q^2,\mu)$, where $g_\perp^{\mu\nu}$ is the metric transverse to the beam and jet collinear directions n_B, n_J of the SCET operator,

$$g_\perp^{\mu\nu} = g^{\mu\nu} - \frac{n_B^\mu n_J^\nu + n_J^\mu n_B^\nu}{n_B \cdot n_J}, \tag{24}$$

satisfying $g_\perp^{\mu\nu} n_{B\nu} = g_\perp^{\mu\nu} n_{J\nu} = 0$ by virtue of $n_B^2 = n_J^2 = 0$. At leading power $n_B \| n$ and $n_J \| \bar{n}$ [the directions of q_B, q_J], with $n \cdot \bar{n} = 2$. The longitudinal pair spans the same plane as $\{n, \bar{n}\}$: explicitly, $U^\mu = \frac{1}{2}(n^\mu + \bar{n}^\mu)$ and $Z^\mu = \frac{1}{2}(n^\mu - \bar{n}^\mu)$, so $\frac{1}{2}(n^\mu \bar{n}^\nu + \bar{n}^\mu n^\nu) = U^\mu U^\nu - Z^\mu Z^\nu$ and the completeness relation (10) collapses the transverse metric to

$$g_\perp^{\mu\nu} = -(X^\mu X^\nu + Y^\mu Y^\nu) = -2x w_2^{\mu\nu}. \tag{25}$$

The leading hard tensor is thus purely transverse and isotropic in the X-Y plane, proportional to $w_2^{\mu\nu}$ alone. Applying the projectors $\mathcal{P}_i$ then feeds it into $F_2^{\rm gap}$ alone:

$$F_L^{\rm gap} = F_3^{\rm gap} = F_4^{\rm gap} = 0 \tag{26}$$

exactly at leading power. The first nonzero $F_{L,3,4}^{\rm gap}$ are suppressed by powers of λ_t relative to $F_2^{\rm gap}$. The vanishing of $F_{3,4}^{\rm gap}$ is manifest in Eq. (25): $g_\perp^{\mu\nu}$ contains neither the X-Y anisotropy $(X^\mu X^\nu - Y^\mu Y^\nu)$ nor the U-X mixing $(U^\mu X^\nu + X^\mu U^\nu)$ that define $w_3^{\mu\nu}$ and $w_4^{\mu\nu}$.

Identifying the two sectors—In practice, to analyze gapped hard scattering in Monte Carlo or experiments, we must choose how we partition a multiparticle state between p_X and p'. Extracting the hadron plane—and hence the azimuth ϕ carrying the discriminating structure functions—requires an operational rule assigning each particle to a sector. It is convenient to choose DIS 1-jettiness τ_1 [14,16,54] as our partition (alternative rules

are reviewed in Sec. 2.3 of [36]) due to the close relationship between its factorization and Eq. (22). We have

$$\tau_1 = \frac{2}{Q^2}\sum_i \min\{q_{X_T}\cdot p_i, q_{X_C}\cdot p_i\}, \tag{27}$$

with lightlike reference vectors $q_{X_T} = (\omega_{X_T}/2)n_B$ (beam) and $q_{X_C} = (\omega_{X_C}/2)n_J$ (current). Each particle joins the sector with the smaller product, partitioning the final state at a boundary rapidity $\eta_0 = \frac{1}{2}\ln(\omega_{X_T}/\omega_{X_C})$,

$$p_X = \sum_{i\in\mathcal{H}_{X_C}} p_i, \qquad p' = \sum_{i\in\mathcal{H}_{X_T}} p_i. \tag{28}$$

The symmetric choice $\omega_{X_C} = \omega_{X_T}$ is the standard hemisphere partition in the Breit frame. Note that τ_1 parallels the role of β in the diffractive factorization Eq. (22), as explained in Supplemental Material [45].

The vanishing of $F^{\text{gap}}_{L,3,4}$ in Eq. (26) is independent of our choice of sector partition in Eq. (28). $H^{\mu\nu} = -g^{\mu\nu}_\perp H(Q^2,\mu)$ is fixed by the collinear directions n_B, n_J, not by the boundary; thus, it remains X-Y isotropic for any partition. At leading power, the boundary enters *only* the soft function S in Eq. (22): the collinear sectors sit at large rapidity, far from any finite η_0, so displacing the boundary reassigns only wide-angle soft radiation, and the soft function reduces to the DIS hemisphere soft function with rescaled arguments. In the gapped dijet limit, the reference directions align with the Breit-frame light-cone axes, $n_J \to \bar{n}$ (current) and $n_B \to n$ (beam) with $n_J\cdot n_B \to 2$, so that $\mathcal{H}_{X_C}$ and $\mathcal{H}_{X_T}$ become the $\bar{n}$- and n-collinear sectors of the factorization.

At leading power, Eq. (22) holds to all orders in α_s: higher-order α_s corrections modify only the scalar functions H, $\mathcal{B}$, J, S, and never generate an X-Y anisotropy, so $F^{\text{gap}}_{L,3,4} = 0$ holds for the resummed leading-power result at any order. A nonzero $F^{\text{gap}}_{L,3,4}$ in gapped hard scattering can therefore arise only beyond leading power—from subleading-power corrections carrying the anisotropic structures absent from $g^{\mu\nu}_\perp$, or from $\mathcal{O}(\alpha_s)$ real radiation outside the two-jet configuration entering through fixed-order matching [55–61]. For example, spin correlations due to gluon splitting in an additional gluon jet could induce azimuthal dependence. At $\mathcal{O}(\alpha_s)$ such modulations are known to scale as powers of $p'_\perp/Q \sim \lambda_t$ [59,62], and we find below, numerically, that the total effect of these $\mathcal{O}(\alpha_s)$ corrections does not notably diminish our ability to discriminate between hard and diffractive events; see Fig. 2. Any surviving azimuthal dependence is genuinely a diffractive signature. In particular, the gapped-hard modulations F^{gap}_3 $(\cos 2\phi)$ and F^{gap}_4 $(\cos\phi)$ of Eq. (14) switch off as $\beta \to 1$, as we show with RAPGAP below.

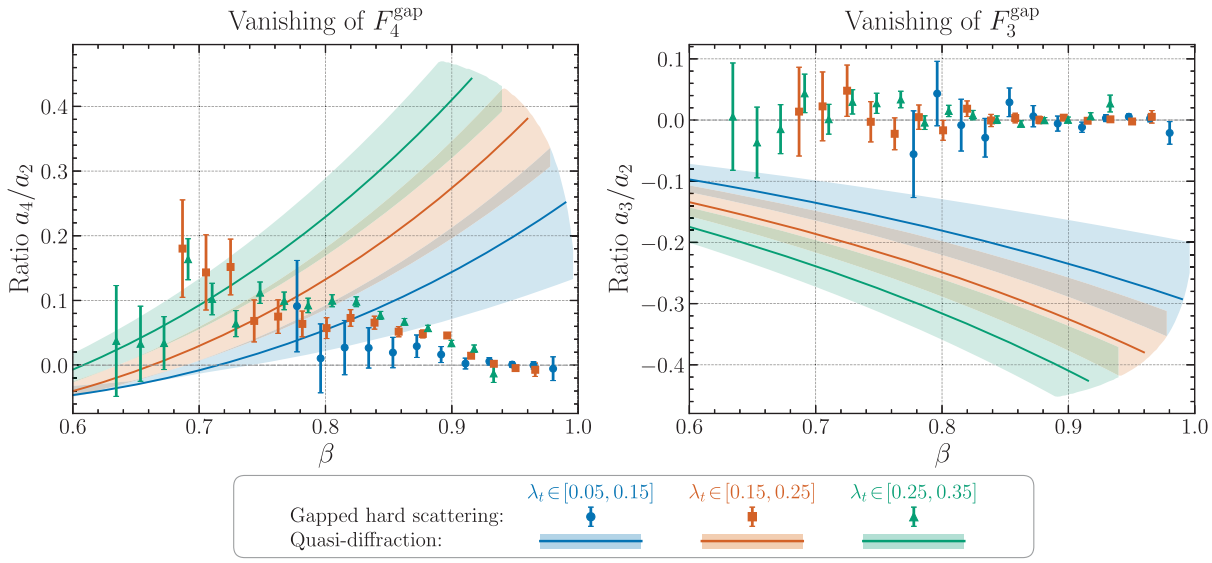


FIG. 2. Ratios involving F^{gap}_4 (left) and F^{gap}_3 (right), for gapped hard scattering (points) and quasi-diffraction (bands). Specifically, we plot the ratios $a_{3,4}/a_2 \propto F^{\text{gap}}_{3,4}/(c_2F^{\text{gap}}_2 + c_LF^{\text{gap}}_L)$ in Eq. (29), where $c_{2/L}$ indicates the y-dependent coefficients in Eq. (14). Ratios are plotted against β in narrow windows of $x \in (0.02, 0.04)$ and $Q^2 \in (800, 1000)$ GeV^2. Gapped hard scattering data are obtained from RAPGAP, as described in the text; they are horizontally offset within each β bin for visibility. They give a very different shape for the distributions than quasi-diffraction. Because each λ_t slice is kinematically confined to a limited β range (small λ_t favoring large β), bins with insufficient statistics for a reliable ϕ fit are not shown. The bands span the leading-power quasi-diffractive prediction of Ref. [36] over the λ_t range of each slice and the x window (at $Q^2 = 900$ GeV^2), with the central line at the midpoints. We use bands to emphasize that quasi-diffraction provides a heuristic but not fully precise comparison between hard and forward gapped scattering, as it reflects color-nonsinglet contributions.

Simulations—We examine our gapped hard scattering analysis with the Monte Carlo generator RAPGAP [35], fitting to the unpolarized azimuthal decomposition

$$d\sigma/d\phi = a_2 + a_4 \cos\phi + a_3 \cos 2\phi. \tag{29}$$

Comparing Eqs. (29) and (14), we have $a_{3,4} \propto F_{3,4}^{\rm gap}$ and $a_2 \propto [1 - y + (y^2/2)]F_2^{\rm gap} - (y^2/2)F_L^{\rm gap}$. We use the combination a_2 because the single $\sqrt{s}$ value we use cannot separate $F_2^{\rm gap}$ and $F_L^{\rm gap}$.

We generate gapped hard scattering in RAPGAP with the full $\mathcal{O}(\alpha_s)$ DIS matrix elements. This is essential: the discriminating modulations are genuine $\mathcal{O}(\alpha_s)$ matrix-element effects. For every event, we split the final state into the p' and p_X hemispheres through the τ_1 partition with the Breit hemisphere choice $\eta_0 = 0$ in Eq. (27), and form the invariants of Eq. (1) directly from the resulting sector momenta.

Figure 2 is our central simulation result. We work at the HERA energy $\sqrt{s} = 319$ GeV in the narrow window $x \in (0.02, 0.04)$, $Q^2 \in (800, 1000)$ GeV^2, so that $y = Q^2/(xs)$ is effectively fixed. We bin in (β, λ_t) and fit the ϕ distribution separately in each of the 45 bins. The fits are good: the χ^2 per degree of freedom has a median of 0.96 and lies between 0.8 and 1.3 in 68% of the bins.

We plot ratios $a_{3,4}/a_2$ to facilitate comparison of gapped hard scattering to diffraction, for which only structure function ratios $F_i^{\rm quasi}/F_2^{\rm quasi}$ are currently available. (Quasi-diffraction refers to the sizable subset of forward gapped processes mediated by color-nonsinglet exchange [36].) We check that leading-order or shower-only generators (e.g., Pythia 8 [63]) give $F_4^{\rm gap}$ consistent with zero even where they reproduce the β and λ_t distributions qualitatively, so the modulation reflects the azimuthal interference of the $\mathcal{O}(\alpha_s)$ amplitude rather than the bulk kinematics, consistent with the $\cos\phi$ modulations seen in inclusive DIS at HERA [64,65].

Both hard modulations $a_{3,4}/a_2$ fall to zero as $\beta \to 1$, realizing the leading-power result $F_3^{\rm gap} = F_4^{\rm gap} = 0$: the azimuthal signal switches off precisely where the rapidity gap is largest. The bands show the quasi-diffractive prediction of Ref. [36], which instead stays nonzero and grows toward $\beta \to 1$. However, the comparison is not one-to-one—Ref. [36] predicts these ratios only for the color-nonsinglet quasi-diffractive background, not including color-singlet diffraction. Our conclusion is independent of this fact; the leading-power result is that hard scattering supplies *no* $F_L^{\rm gap}, F_3^{\rm gap}, F_4^{\rm gap}$ as $\beta \to 1$, so *any* azimuthal or longitudinal signal surviving in the large-gap region is necessarily of diffractive origin—the hard background is absent, not merely subdominant.

Conclusions and outlook—We factorize rapidity-gapped hard scattering in DIS, and show that at leading power its hard tensor is purely transverse, $H^{\mu\nu} \propto g_\perp^{\mu\nu} \propto w_2^{\mu\nu}$. As a consequence the longitudinal and azimuthal structure functions vanish exactly, $F_L^{\rm gap} = F_3^{\rm gap} = F_4^{\rm gap} = 0$, independently of the sector partition and to all orders in α_s at leading power. Any azimuthal or longitudinal modulation surviving in the large-gap region is therefore not a hard-scattering background but a genuine diffractive signature. RAPGAP simulations are consistent with hard modulations switching off as $\beta \to 1$, realizing this result. This provides evidence that these structure functions are a clean, model-independent handle for separating diffraction from its hard background at the EIC. Natural next steps include extending the analysis to subleading power—where the first nonzero $F_{L,3,4}^{\rm gap}$ appear, quantifying the residual hard contamination—to the polarized and nuclear cases relevant for the EIC program, and to the LHC case [66].

Acknowledgments—We thank I. Stewart for helpful discussions. S. T. S. appreciates the hospitality of Harvard, MIT, and Washington University in St. Louis during work on this manuscript. This work was supported by the U.S. Department of Energy, Office of Science, through the Office of Nuclear Physics, and the LDRD Program at Los Alamos National Laboratory under Projects No. 20230857PRD2, No. 20240786PRD1 and No. 20250214ER. LANL is operated by Triad National Security, LLC, for the National Nuclear Security Administration of the U.S. Department of Energy under Contract No. 89233218CNA000001.

Data availability—There are no publicly available research data or software supporting this manuscript. Requests for further information or data should be sent to the authors.

[1] R. Abdul Khalek *et al.*, Science requirements and detector concepts for the electron-ion collider: EIC yellow report, Nucl. Phys. **A1026**, 122447 (2022).
[2] E. L. Feinberg and I. Pomerančuk, High energy inelastic diffraction phenomena, Il Nuovo Cimento (1955–1965) **3**, 652 (1956).
[3] G. F. Chew and S. C. Frautschi, Principle of equivalence for all strongly interacting particles within the S matrix framework, Phys. Rev. Lett. **7**, 394 (1961).
[4] L. Frankfurt, V. Guzey, A. Stasto, and M. Strikman, Selected topics in diffraction with protons and nuclei: Past, present, and future, Rep. Prog. Phys. **85**, 126301 (2022).
[5] R. J. Glauber, Cross sections in deuterium at high energies, Phys. Rev. **100**, 242 (1955).
[6] V. N. Gribov, Glauber corrections and the interaction between high-energy hadrons and nuclei, Sov. Phys. JETP **29**, 483 (1969).
[7] M. Hentschinski *et al.*, White paper on forward physics, BFKL, saturation physics and diffraction, Acta Phys. Pol. B **54**, 3 (2023).

[8] R. Engel, D. Heck, and T. Pierog, Extensive air showers and hadronic interactions at high energy, Annu. Rev. Nucl. Part. Sci. **61**, 467 (2011).

[9] K. Akiba *et al.* (LHC Forward Physics Working Group), LHC forward physics, J. Phys. G **43**, 110201 (2016).

[10] V. A. Khoze, A. D. Martin, and M. G. Ryskin, Prospects for new physics observations in diffractive processes at the LHC and Tevatron, Eur. Phys. J. C **23**, 311 (2002).

[11] M. G. Albrow, T. D. Coughlin, and J. R. Forshaw, Central exclusive particle production at high energy hadron colliders, Prog. Part. Nucl. Phys. **65**, 149 (2010).

[12] J. L. Feng *et al.*, The forward physics facility at the high-luminosity LHC, J. Phys. G **50**, 030501 (2023).

[13] A. Tumasyan *et al.* (CMS and TOTEM Collaborations), A search for new physics in central exclusive production using the missing mass technique with the CMS detector and the CMS-TOTEM precision proton spectrometer, Eur. Phys. J. C **83**, 827 (2023).

[14] D. Kang, C. Lee, and I. W. Stewart, Using 1-jettiness to measure 2 jets in DIS 3 ways, Phys. Rev. D **88**, 054004 (2013).

[15] M. Dasgupta and G. P. Salam, Event shapes in e^+e^- annihilation and deep inelastic scattering, J. Phys. G **30**, R143 (2004).

[16] Z.-B. Kang, S. Mantry, and J.-W. Qiu, N-jettiness as a probe of nuclear dynamics, Phys. Rev. D **86**, 114011 (2012).

[17] C. F. Berger, C. Marcantonini, I. W. Stewart, F. J. Tackmann, and W. J. Waalewijn, Higgs production with a central jet veto at NNLL + NNLO, J. High Energy Phys. 04 (2011) 092.

[18] A. Banfi, G. P. Salam, and G. Zanderighi, NLL + NNLO predictions for jet-veto efficiencies in Higgs-boson and Drell-Yan production, J. High Energy Phys. 06 (2012) 159.

[19] T. Becher and M. Neubert, Factorization and NNLL resummation for Higgs production with a jet veto, J. High Energy Phys. 07 (2012) 108.

[20] F. J. Tackmann, J. R. Walsh, and S. Zuberi, Resummation properties of jet vetoes at the LHC, Phys. Rev. D **86**, 053011 (2012).

[21] A. Banfi, P. F. Monni, G. P. Salam, and G. Zanderighi, Higgs and Z-boson production with a jet veto, Phys. Rev. Lett. **109**, 202001 (2012).

[22] X. Liu and F. Petriello, Resummation of jet-veto logarithms in hadronic processes containing jets, Phys. Rev. D **87**, 014018 (2013).

[23] T. T. Jouttenus, I. W. Stewart, F. J. Tackmann, and W. J. Waalewijn, Jet mass spectra in Higgs boson plus one jet at next-to-next-to-leading logarithmic order, Phys. Rev. D **88**, 054031 (2013).

[24] I. W. Stewart, F. J. Tackmann, J. R. Walsh, and S. Zuberi, Jet p_T resummation in Higgs production at NNLL′ + NNLO, Phys. Rev. D **89**, 054001 (2014).

[25] D. Y. Shao, C. S. Li, and H. T. Li, Resummation prediction on Higgs and vector boson associated production with a jet veto at the LHC, J. High Energy Phys. 02 (2014) 117.

[26] Y. Li and X. Liu, High precision predictions for exclusive VH production at the LHC, J. High Energy Phys. 06 (2014) 028.

[27] J. R. Forshaw, A. Kyrieleis, and M. H. Seymour, Super-leading logarithms in non-global observables in QCD, J. High Energy Phys. 08 (2006) 059.

[28] T. Becher, M. Neubert, D. Y. Shao, and M. Stillger, Factorization of non-global LHC observables and resummation of super-leading logarithms, J. High Energy Phys. 12 (2023) 116.

[29] J.-W. Qiu and Z. Yu, Single diffractive hard exclusive processes for the study of generalized parton distributions, Phys. Rev. D **107**, 014007 (2023).

[30] J.-W. Qiu, N. Sato, and Z. Yu, Unified and optimal frame choice for generalized parton distributions, Phys. Rev. D **111**, 094014 (2025).

[31] J.-H. Ee, D. Kang, C. Lee, and I. W. Stewart, Precision DIS thrust predictions for HERA and EIC, J. High Energy Phys. 07 (2025) 240.

[32] A. Aktas *et al.* (H1 Collaboration), Measurement and QCD analysis of the diffractive deep-inelastic scattering cross-section at HERA, Eur. Phys. J. C **48**, 715 (2006).

[33] G. Aad *et al.* (ATLAS Collaboration), Rapidity gap cross sections measured with the ATLAS detector in pp collisions at $\sqrt{s} = 7$ TeV, Eur. Phys. J. C **72**, 1926 (2012).

[34] G. Aad *et al.* (ATLAS Collaboration), Measurement of differential cross sections for single diffractive dissociation in $\sqrt{s} = 8$ TeV pp collisions using the ATLAS ALFA spectrometer, J. High Energy Phys. 02 (2020) 042; 10 (2020) 182(E).

[35] H. Jung, Hard diffractive scattering in high-energy ep collisions and the Monte Carlo generator RAPGAP, Comput. Phys. Commun. **86**, 147 (1995).

[36] K. Lee, S. T. Schindler, and I. W. Stewart, Effective field theory factorization for diffraction, J. High Energy Phys. 11 (2025) 157.

[37] T. Arens, O. Nachtmann, M. Diehl, and P. V. Landshoff, Some tests for the helicity structure of the pomeron in ep collisions, Z. Phys. C **74**, 651 (1997).

[38] F. D. Aaron *et al.* (H1 Collaboration), Measurement of the diffractive longitudinal structure function F_L^D at HERA, Eur. Phys. J. C **71**, 1836 (2011).

[39] S. Chekanov *et al.* (ZEUS Collaboration), Dissociation of virtual photons in events with a leading proton at HERA, Eur. Phys. J. C **38**, 43 (2004).

[40] C. W. Bauer, S. Fleming, and M. E. Luke, Summing Sudakov logarithms in $B \to X_s\gamma$ in effective field theory, Phys. Rev. D **63**, 014006 (2000).

[41] C. W. Bauer, S. Fleming, D. Pirjol, and I. W. Stewart, An effective field theory for collinear and soft gluons: Heavy to light decays, Phys. Rev. D **63**, 114020 (2001).

[42] C. W. Bauer and I. W. Stewart, Invariant operators in collinear effective theory, Phys. Lett. B **516**, 134 (2001).

[43] C. W. Bauer, D. Pirjol, and I. W. Stewart, Soft collinear factorization in effective field theory, Phys. Rev. D **65**, 054022 (2002).

[44] I. Z. Rothstein and I. W. Stewart, An effective field theory for forward scattering and factorization violation, J. High Energy Phys. 08 (2016) 025.

[45] See Supplemental Material at http://link.aps.org/supplemental/10.1103/7jkz-3r9q for the complete derivation of the fully differential factorization formula, which includes Refs. [46–53].

[46] T. Becher and M. Neubert, Toward a NNLO calculation of the $\bar{\mathrm{B}} \to \mathrm{X}_{(\mathrm{s})}\gamma$ decay rate with a cut on photon energy. II.

Two-loop result for the jet function, Phys. Lett. B **637**, 251 (2006).
[47] A. Jain, M. Procura, and W. J. Waalewijn, Fully unintegrated parton distribution and fragmentation functions at perturbative k_T, J. High Energy Phys. 04 (2012) 132.
[48] R. Kelley, M. D. Schwartz, R. M. Schabinger, and H. X. Zhu, The two-loop hemisphere soft function, Phys. Rev. D **84**, 045022 (2011).
[49] P. F. Monni, T. Gehrmann, and G. Luisoni, Two-loop soft corrections and resummation of the thrust distribution in the dijet region, J. High Energy Phys. 08 (2011) 010.
[50] A. Hornig, C. Lee, I. W. Stewart, J. R. Walsh, and S. Zuberi, Non-global structure of the $\mathcal{O}(\alpha_s^2)$ dijet soft function, J. High Energy Phys. 08 (2011) 054; 10 (2017) 101(E).
[51] A. V. Manohar, Deep inelastic scattering as $x \to 1$ using soft collinear effective theory, Phys. Rev. D **68**, 114019 (2003).
[52] A. Idilbi, X.-d. Ji, and F. Yuan, Resummation of threshold logarithms in effective field theory for DIS, Drell-Yan and Higgs production, Nucl. Phys. **B753**, 42 (2006).
[53] T. Becher, M. Neubert, and B. D. Pecjak, Factorization and momentum-space resummation in deep-inelastic scattering, J. High Energy Phys. 01 (2007) 076.
[54] A. Dotson, J.-H. Ee, C. Lee, Y. Makris, and J. Terry, Centauric 1-jettiness in DIS and universal power corrections, J. High Energy Phys. 09 (2026) 224.
[55] H. Georgi and H. D. Politzer, Clean tests of QCD in μp scattering, Phys. Rev. Lett. **40**, 3 (1978).
[56] R. N. Cahn, Azimuthal dependence in leptoproduction: A simple parton model calculation, Phys. Lett. **78B**, 269 (1978).
[57] J. Cleymans, Angular correlations in lepton-hadron scattering, Phys. Rev. D **18**, 954 (1978).
[58] G. Kopp, R. Maciejko, and P. M. Zerwas, Angular asymmetries in hadron distributions of neutrino-nucleon reactions in quantum chromodynamics, Nucl. Phys. **B144**, 123 (1978).
[59] A. Mendez, QCD predictions for semiinclusive and inclusive leptoproduction, Nucl. Phys. **B145**, 199 (1978).
[60] A. König and P. Kroll, A realistic calculation of the azimuthal asymmetry in semiinclusive deep inelastic scattering, Z. Phys. C **16**, 89 (1982).
[61] J.-g. Chay, S. D. Ellis, and W. J. Stirling, Azimuthal asymmetry in lepton-photon scattering at high energies, Phys. Rev. D **45**, 46 (1992).
[62] A. Bacchetta, D. Boer, M. Diehl, and P. J. Mulders, Matches and mismatches in the descriptions of semi-inclusive processes at low and high transverse momentum, J. High Energy Phys. 08 (2008) 023.
[63] C. Bierlich *et al.*, A comprehensive guide to the physics and usage of Pythia 8.3, SciPost Phys. Codebases **2022**, 8 (2022).
[64] J. Breitweg *et al.* (ZEUS Collaboration), Measurement of azimuthal asymmetries in deep inelastic scattering, Phys. Lett. B **481**, 199 (2000).
[65] S. Chekanov *et al.* (ZEUS Collaboration), Study of the azimuthal asymmetry of jets in neutral current deep inelastic scattering at HERA, Phys. Lett. B **551**, 226 (2003).
[66] P. B. Aretz, K. Lee, S. T. Schindler, and I. W. Stewart, Factorization of elastic, single, and double diffractive pp scattering, arXiv:2607.07788.